

PAPER



Cite this: *J. Mater. Chem. C*, 2017,
5, 5787

Received 18th January 2017,
Accepted 10th April 2017

DOI: 10.1039/c7tc00293a

rsc.li/materials-c

Vapor phase organic chemistry to deposit
conjugated polymer films on arbitrary substrates†

Nongyi Cheng,‡^{ab} Lushuai Zhang,‡^a Jae Joon Kim^{ac} and Trisha L. Andrew^{id} *^{ac}

Coating textured, high surface area substrates, such as paper and textiles, with conjugated polymer films is challenging. Selected vapor deposition techniques allow for the film forming process to be largely divorced of substrate properties, such as surface energy and surface roughness, and have the potential to yield conformal coatings. However, reliable vapor deposition techniques with which to fabricate structurally-diverse conjugated polymer films do not exist. Here, we report two vapor deposition chambers that, combined, allow for *in situ* vapor phase polymerization of a representative selection of common conjugated monomers. Conformal coating of highly disordered, high surface area three-dimensional substrates, including a cotton towel and corduroy fabric, with either conductive PEDOT or poly(thieno[3,2-*b*]thiophene) films of precisely-controlled thickness is described.

Introduction

Polymeric organic semiconductors display unique materials properties, such as flexibility,¹ stretchability,² transparency,³ and low density,⁴ which allow unmatched control over processing conditions⁵ and make possible nontraditional electronic⁶ and optoelectronic⁷ device architectures on arbitrary substrates. Currently, many researchers are endeavoring to use the advantageous mechanical properties of conjugated polymer films to create flexible,⁸ stretchable⁹ and/or skin-mountable devices.¹⁰ Intense research efforts over the past three decades have yielded a large library of monomers for conducting and semiconducting polymers,¹¹ as well as a strong understanding of the correlations between chemical structure, processing conditions,¹² optoelectronic characteristics,¹³ and condensed phase morphology.¹⁴

Nonetheless, the ability to conformally coat textured, high surface area substrates with conjugated polymer films remains unmastered. Indeed, the “coatability” of various materials remains a major consideration in choosing potential substrates for next-generation devices, such as flexible and/or wearable electronics¹⁵ and smart textiles.¹⁶ Fabrics and threads/yarns, in particular, are demanding substrates onto which to deposit a

conjugated polymer film because their surfaces are densely textured and display roughness over a wide range of length scales (micron length scales for fibers, micron-millimeter length scales for threads/yarns and millimeter-centimeter length scales for woven and knitted fabrics).¹⁷ To date, dipcoating,¹⁸ *in situ* solution polymerization,¹⁹ solution-phase surface grafting²⁰ or electropolymerization²¹ are primarily used to coat fibers with conjugated polymer films. Although these methods afford functional fibers for academic research, the coatings thus obtained are often non-uniform²² and susceptible to mechanically-induced degradation and abrasion.²³ Due to these limitations, the use of specialty or niche fibers with uncommonly smooth surfaces, such as diamond-tip extruded stainless steel thread or extruded fiberglass, are required to produce functional optoelectronic devices.²⁴

Reactive vapor coating methods, such as atomic layer deposition²⁵ and chemical vapor deposition,²⁶ are known to reliably and conformally deposit thin films onto a diverse range of substrates, irrespective of surface chemistry/composition, surface energy and surface roughness/topography. However, thus far, the chemistry underlying these techniques is only established broadly for inorganic precursors.²⁵ In comparison, reactive vapor deposition of few organic polymers has been demonstrated²⁷ and an even narrower set of conjugated polymer films are deposited using vapor phase techniques.²⁸

Here, we report two vapor deposition chambers that, combined, allow for *in situ* vapor phase oxidative polymerization of common conjugated monomers. Conformal surface coating of densely textured, high-surface-area substrates, including a cotton towel and corduroy fabric, with either conductive polymer films, such as poly(3,4-ethylenedioxythiophene) (PEDOT), or semiconducting polymer films, such as poly(thieno[3,2-*b*]thiophene) (PTT), is described. We also show that similarly conformal conjugated

^a Department of Chemistry, University of Massachusetts Amherst, Amherst, MA 01003, USA. E-mail: tandrew@umass.edu

^b Department of Chemistry, University of Wisconsin-Madison, Madison, WI 53706, USA

^c Department of Polymer Science and Engineering, University of Massachusetts Amherst, Amherst, MA 01003, USA

† Electronic supplementary information (ESI) available: Absorbance spectra, XPS data, sample photographs. See DOI: 10.1039/c7tc00293a

‡ These authors contributed equally to this work.

polymer coatings on textured substrates cannot be achieved using traditional solution processing methods.

Experimental

Materials and methods

All chemicals were purchased from Sigma Aldrich and used without further purification. Cyclic voltammetry (CV) measurements were performed with a Wavenow potentiostat, in 0.1 M tetrabutylammonium hexafluorophosphate (TBAPF₆) in dichloromethane, with Ag/AgNO₃ in acetonitrile as a reference electrode. X-ray photoelectron spectroscopy (XPS) was carried out with a Physical Electronics Inc. 5000 Series spectrophotometer. Scanning electron microscopy (SEM) was performed using a FESEM Magellan 400. Ultraviolet photoelectron spectroscopy (UPS) was carried out using an Omicron SPHERA hemispherical analyzer and a He I light source (21.2 eV). Samples for UPS measurements were prepared on ITO/glass substrates that were cleaned as follows before use: sonicated in detergent solution, rinsed in DI water followed by acetone for 5 min, dipped into boiling isopropanol for 5 min (2×), and then treated with UV-ozone for 15 min. Conductivities were calculated from resistivity measurements using a home-built four-point probe test station. Film thicknesses were measured on a Veeco Dektak 150 profilometer.

Vapor phase polymerization with a cubic chamber (chamber 1)

Vapor phase polymerization of monomers **EDOT**, **MT** and **DMT** was carried out in a custom-built cube-shaped stainless steel chamber (Fig. 1a) adapted from previous reports.³⁰ The pressure inside the chamber was tuned between 100–500 mTorr by introducing and controlling an argon gas flow, in addition to the monomer and oxidant flux. A solid oxidant, typically FeCl₃, was sublimed inside the chamber using a Luxel crucible heater. Monomers were introduced into the evacuated chamber in the vapor phase *via* a side inlet. For poly(3-methylthiophene) (**PMT**) or poly(3,4-dimethylthiophene) (**PDMT**) deposition, a glass ampule containing the volatile liquid monomer (**MT** or **DMT**, respectively) was connected to the chamber, and the monomer vapor was introduced into the chamber at a constant rate of

20 sccm using a mass flow controller. For **PEDOT** deposition, a glass ampule containing **EDOT** was heated with resistive heating tape to 80 °C and the monomer vapor flow into the chamber was controlled by a needle valve. The substrate stage inside the chamber was maintained at 30 °C for **PMT** and **PDMT** deposition and varied between 30–80 °C for **PEDOT** deposition. Substrates such as glass slides, ITO coated glass, paper and fabrics were all successfully tested. After vapor deposition, the coated substrates were rinsed with copious amounts of methanol or 1% by volume conc. H₂SO₄ in methanol under air to remove residual monomer and oxidant from the polymer films. Previous reports confirmed *via* XPS that residual iron salts are completely removed from the polymer films thus obtained after rinsing.³¹

The thickness of the growing polymer film inside the chamber was monitored in real time by a quartz crystal microbalance (QCM) sensor situated near the substrate stage. The total deposition rate and film thickness values reported by the QCM sensor during vapor deposition arise from both the polymer film and unreacted monomer/oxidant being deposited onto the sensor surface. Thickest polymer films were obtained after rinsing when the monomer and oxidant flow rates were matched during deposition. Unreacted monomers or oxidants remain trapped in the films if the monomer/oxidant flow rates are mismatched, which are leached out of the film during rinsing, leading to significantly lower film thicknesses than measured by the QCM sensor during deposition. A corrective tooling factor to account for this discrepancy was obtained as follows. Silicon substrates were coated with films of varying thickness (“QCM reported”) at three different monomer:oxidant flow rate ratios, rinsed with H₂SO₄/methanol, and the resulting film thickness (“actual thickness”) measured using a profilometer. A tooling factor was obtained by taking the ratio of the actual film thickness after rinsing to the thickness reported by the QCM sensor during deposition. The tooling factor was found to be 0.5 for all monomer:oxidant flow rate ratios. Taking this correction into account, typical polymer growth rates on any surface were 12–20 nm min⁻¹ for substrate stage temperatures between 30 °C to 50 °C. Film growth was slightly slower at higher substrate temperatures: 10–15 nm min⁻¹.

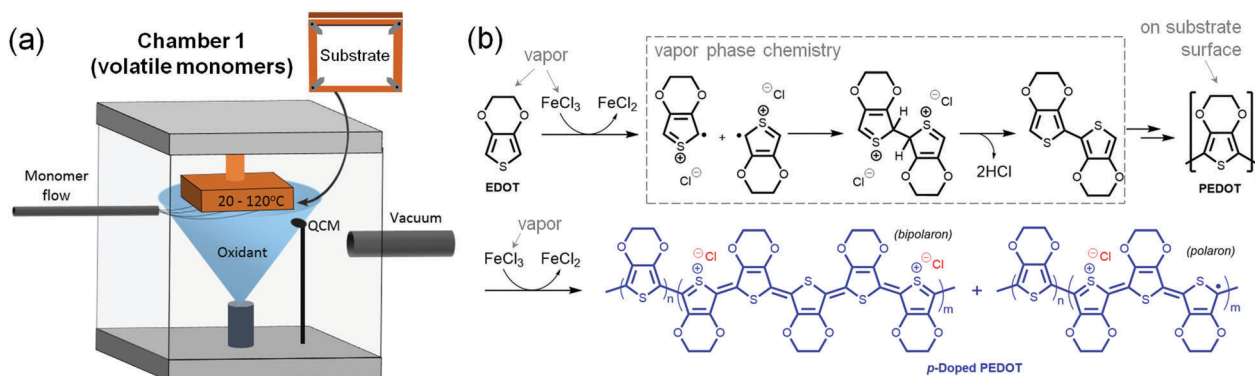


Fig. 1 (a) Schematic cartoon of a cube-shaped vapor deposition chamber. (b) Reaction scheme of oxidative polymerization of EDOT and the bipolaron and polaron form of the resulting polymer.

Vapor phase polymerization with a tubular chamber (chamber 2)

Vapor phase polymerization of solid and low-volatility monomers was carried out in a custom-built tubular quartz chamber (Fig. 2a) containing up to three side inlets. Monomers and oxidants were vaporized from either glass ampoules or tungsten crucibles heated with resistive heating tape, and the respective vapors introduced into the tube chamber *via* different side inlets. The distance between the monomer inlet and the oxidant crucible/inlet was 5 inches for all polymerizations. The process pressure was maintained close to 120 mTorr for all depositions. Substrates such as glass slides, ITO coated glass, paper and fabrics were all successfully tested. To obtain polymers using solid FeCl_3 as the oxidant, a sequential heating algorithm was followed. First, the oxidant and substrate regions (see Fig. 2a) were heated to 170 °C and 80 °C, respectively, for 8 min. Second, the glass ampule containing the monomer was heated and the resulting monomer vapor was introduced into the tube. The heating temperatures for **ProDOT**, **DMProDOT**, **HMEDOT**, **TT**, **BiT**, and **TerT** were 70 °C, 70 °C, 120 °C, 90 °C, 35 °C, and 100 °C, respectively. For **PEDOT** obtained using gaseous Br_2 as the oxidant, the heating temperature for the monomer was 70 °C and the substrates and oxidant were maintained at room temperature. After vapor deposition, polymer films were rinsed with copious amounts of methanol under air to remove residual monomer and oxidant. XPS spectra (Fig. S2, ESI†) of PProDOT films before and after rinsing confirm that all residual iron salts were completely rinsed out. Polymer film thicknesses were manually controlled by monitoring reaction times and heating temperatures: silicon substrates were subjected to vapor coating for varying amounts of time at few different

monomer heating temperatures, rinsed with methanol, and the resulting film thicknesses measured with a profilometer to afford film thickness *versus* time curves for each monomer at particular heating temperatures. Under optimized heating conditions, film growth was observed to be linear with time for all monomers and typical growth rates were 10 nm min^{-1} .

Results and discussion

1. Monomers with high vapor pressures

In order to enable vapor phase polymerization of conjugated monomers, our strategy is to, first, focus on monomers (Chart 1) that are known to participate in solution-phase step growth oxidative polymerization reactions³² (or can be reasonably expected to do so) and, second, to concomitantly introduce the two main components of this reaction (monomer, oxidant) into a reaction chamber in the vapor phase.

A schematic cartoon of the stainless steel, cubic chamber (chamber 1) that was initially built for this purpose is shown in Fig. 1a. The chamber design is adapted from previous reports³⁰ on the vapor phase polymerization of **EDOT**. The major components of chamber 1 include: an electrical furnace to uniformly deliver oxidant vapor to a sample stage situated at seven inches above the furnace; a $5 \times 5 \text{ inch}^2$ heated sample stage; an *in situ* quartz crystal microbalance (QCM) sensor to monitor the monomer/oxidant flow rates and thickness of a deposited film in real time; and stainless steel tubing with in-line mass flow controller to transport the monomer vapor from outside of the chamber. Additional noble gases can be introduced into the chamber from a second gas inlet to control

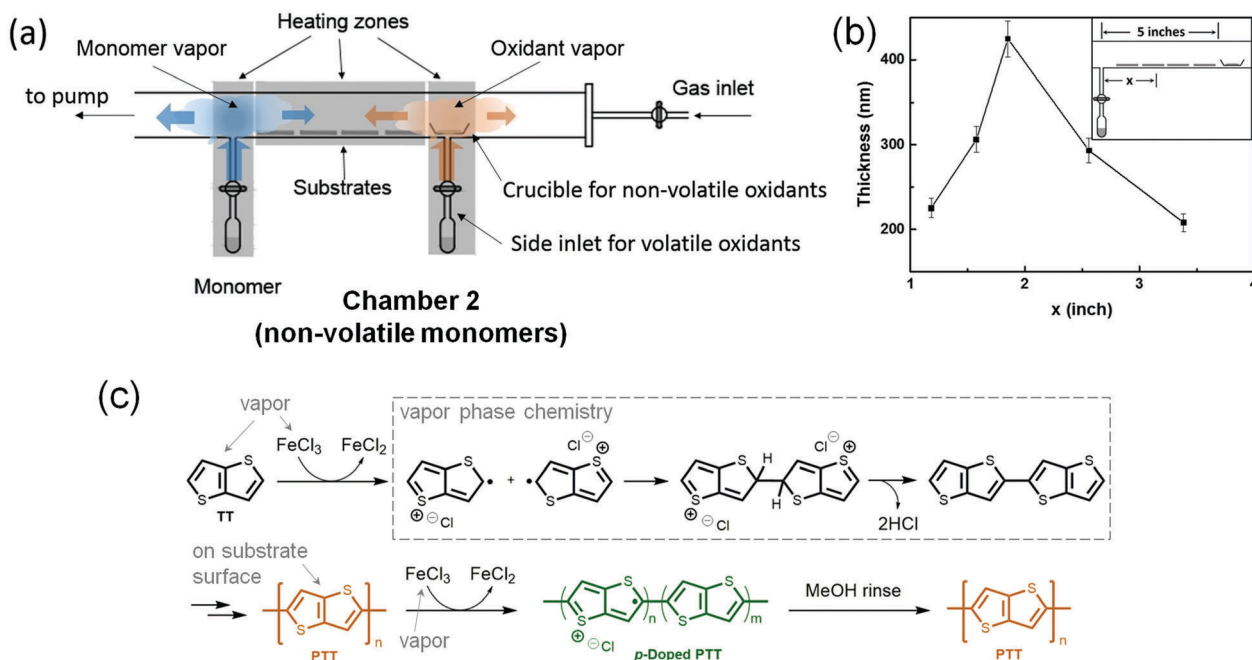


Fig. 2 (a) Schematic cartoon of a tubular vapor deposition chamber. (b) Lateral polymer film thickness profile for the vapor polymerization of ProDOT in chamber 2. Films were grown on 1×1 inch glass slides for 15 minutes prior to measurement. (c) Reaction scheme of oxidative polymerization of thieno[3,2-*b*]thiophene (TT) and doped form of the resulting polymer.

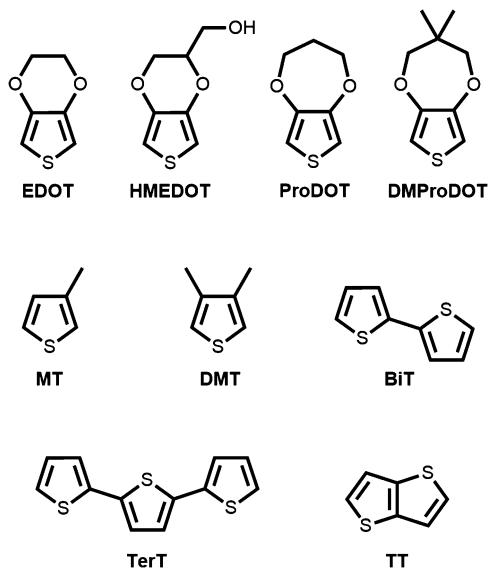


Chart 1 Structures of monomers subjected to vapor phase oxidative polymerization.

the process pressure. Vapor phase oligomerization is expected to occur in the regions where the monomer vapor flux intersects with the conical oxidant vapor plume and the resulting oligomers, which should possess comparatively low kinetic energy, are expected to adhere to any surface placed within these intersectional regions. Heating the sample stage during deposition should impart lateral mobility along the substrate surface to these adsorbed oligomers and, thus, lead to high surface conformality.³³

Three thiophene monomers that are liquids at room temperature, **EDOT**, **MT** and **DMT** (see Table 1), were successfully vapor polymerized in chamber 1 and uniform, four square inch wide films of the corresponding polymers, **PEDOT**, **PMT** and **PDMT**, were deposited with precisely controllable thickness onto glass, ITO-covered glass, silicon wafers, paper and various textiles. Optoelectronic characterization of these films are provided below.

2. Monomers with low vapor pressures

One of the drawbacks of chamber 1 is that only volatile (high vapor pressure) monomers were observed to yield conjugated

Table 1 Physical properties of the monomers subjected to vapor phase oxidative polymerization

Monomer	Physical state	Melting point ^a (°C)	Boiling point ^a (°C)/760 mmHg
MT	Liquid	−69	115
DMT	Liquid	—	144–146 ²⁹
EDOT	Liquid	10.5	193
BiT	Solid	32–33	260
DMPProDOT	Solid	41–46	—
HMEDOT	Solid	42–46	—
TT	Solid	56–58	—
ProDOT	Solid	79–83	—
TerT	Solid	93–95	—

^a Values are from Sigma Aldrich.

polymer films. In the case of nonvolatile monomers, the monomer vapor plume rapidly loses kinetic energy once it is introduced into the chamber. Most of the monomer vapor condenses before it intersects with the oxidant plume and no polymer is observed to be formed on the substrate stage.

For this reason, we designed a new tubular vapor deposition system for polymerization of nonvolatile monomers (chamber 2, Fig. 2a). The central two inch-wide tube is made of quartz and contains three $\frac{1}{4}$ inch side inlets. Monomer and oxidant vapors are introduced into the central tube through two different side inlets. In chamber 2, both the monomer and oxidant sources and vapor inlets are located close together (5 inches). Thus, even if the monomer and/or oxidant molecules display a short mean free path in the gas phase, these vapor plumes have a reasonable chance of intersecting and forming the necessary reactive radical species needed for oligomerization and polymerization.

Another feature of this chamber is that two kinds of oxidants can be readily used: non-volatile oxidants, such as FeCl_3 , and volatile oxidants, such as Br_2 . In the case of non-volatile oxidants, the oxidant is loaded in a crucible and placed inside the tube. In the case of volatile oxidants, the oxidant is loaded in a flask and injected *via* a second needle valve through the second side inlet. Although, in theory, chamber 1 can also accommodate the use of volatile oxidants, in practice, vapor phase polymerizations with bromine were hard to control and reliably reproduce using chamber 1.

The proposed mass transport directions of the monomer and the oxidant vapor are shown as arrows in Fig. 2a. Accordingly, substrates are placed between the monomer inlet and the oxidant crucible. Monomers, substrates and the oxidant are heated by resistive heating tapes with temperature controllers. The monomer flow rate is adjusted with a needle valve and/or by controlling the heating temperature. Unlike chamber 1, chamber 2 lacks an *in situ* QCM sensor and, therefore, polymer film deposition rates and film thicknesses cannot be monitored in real time. Polymer films of a desired thickness are grown by controlling monomer heating temperatures and vapor deposition times. Depending on the monomer, film thicknesses are uniform over a $\frac{3}{4}$ –1 square inch area.

Chamber 2 was used to polymerize six nonvolatile monomers that are solids at room temperature: **ProDOT**, **DMPProDOT**, **HMEDOT**, **TT**, **BiT**, and **TerT** (see Chart 1). These monomers were chosen because they are commonly-found moieties in the repeat units of conjugated polymers and because, together, they span a range of melting points. The corresponding polymers are named as **PProDOT**, **PDMPProDOT**, **PHMEDOT**, **PTT**, **PBiT**, and **PTerT**, respectively. To date, the reactive vapor deposition of these monomers has not been successfully demonstrated. This is the first time that **PTT** has been synthesized.

Iron(III) chloride was used as the oxidant for all six monomers, and Br_2 was also investigated as an oxidant for **EDOT** using chamber 2 (the resulting **PEDOT** film is identified as **Br-PEDOT**). All polymer films thus obtained were amorphous and did not display any significant order peaks (as measured by X-ray diffraction).

For all polymerizations in chamber 2, polymers are formed between the monomer inlet and the oxidant inlet. To better

characterize mass transport in chamber 2, the polymer film thickness at discrete lateral positions along the tube between the monomer and oxidant inlets was measured. Fig. 2b shows the thickness of **PProDOT** films formed on 1×1 inch glass slides placed at discrete lateral positions along the central tube. In general, the thickest polymer film is formed in the middle between the two vapor sources and the polymer film thickness progressively decreases while moving away from the middle in either lateral direction. This observation supports the mass flow arrows depicted in Fig. 2a and reveals that the polymer film thickness can be controlled using both reaction time and the substrate position.

After vapor deposition in either chamber 1 or 2, polymer films were rinsed with methanol to remove the residual monomer, oxidant and metal byproducts. Complete removal of iron salts was confirmed by XPS spectra (Fig. S1–S3, ESI[†]) and has also been proven in previous reports.³¹ Owing to the presence of excess oxidant during the vapor deposition process, the polymer isolated immediately after deposition is p-doped, irrespective of the structure of the starting monomer. However, the post-deposition methanol rinse affects the polymer films in one of two ways: **PEDOT**, **PHMEDOT**, **PProDOT**, and **PDMProDOT** films remain stably p-doped after rinsing, whereas **PMT**, **PDMT**, **PBiT**, **PTerT**, and **PTT** films are effectively de-doped during the rinsing process.

3. Optoelectronic characterization of vapor deposited films

XPS spectra of a 100 nm thick p-doped **PProDOT** film (FeCl_3 oxidant, chamber 2) before and after methanol rinsing confirm that Fe is completely removed upon rinsing with methanol but that chloride counterions remain in the film, indicating that the polymer film remains positively charged after rinsing (Fig. S1 and S2, ESI[†]). The absorption spectra of methanol rinsed **PEDOT**, **PHMEDOT**, **PProDOT** and **PDMProDOT** films (Fig. 3a) confirm that these polymers remain p-doped after rinsing: broad, featureless absorption bands beyond 600 nm that are characteristic of bipolaron and polaron absorption features are observed.³³ Fig. S4a (ESI[†]) details the evolution of these bipolaron and polaron absorption features with varying methanol rinse times for a vapor deposited **PProDOT** film.

In comparison, vapor deposited **PMT**, **PDMT**, **PBiT**, **PTerT**, and **PTT** films are de-doped during the rinsing process and neutral, semiconducting films are obtained after washing. As seen in Fig. 3b, rinsed **PBiT**, **PTT** and **PTerT** films display a dominant peak at 430 nm, which is characteristic of a backbone $\pi \rightarrow \pi^*$ transition,³⁴ but lack the broad near infrared absorption features expected from the polaron species present in p-doped poly(thiophene) derivatives. Fig. S4b (ESI[†]) details the evolution of the absorption spectrum with varying methanol rinse times for a vapor deposited **PTT** film. The unrinsed **PTT** film indeed displays a broad polaron absorption band at 700 nm, confirming that the as-deposited **PTT** film is p-doped. This absorption feature disappears after rinsing in methanol for 10 s, accompanied by an increase in the intensity of the absorption feature at 430 nm indicating that the **PTT** film is effectively de-doped after 10 s of rinsing.

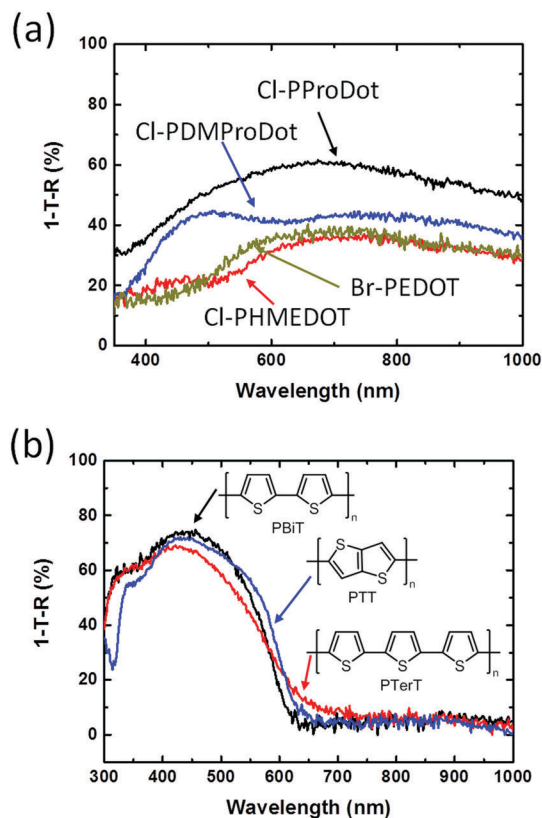


Fig. 3 Absorption spectra, measured as 1-transmittance–reflectance using an integrating sphere, of vapor deposited conjugated polymer films after rinsing with methanol. All films were deposited on glass slides using chamber 2. (a) **Cl-PProDOT**, **Cl-PDMProDOT** and **Cl-PHMEDOT** obtained using FeCl_3 as oxidant, and **Br-PEDOT** obtained using Br_2 as oxidant. (b) **PBiT**, **PTerT**, and **PTT**.

The measured conductivities of 100 nm thick vapor deposited p-doped **PProDOT**, **PDMProDOT**, **PHMEDOT** films are notable: 106, 31.3, and 1.68 S cm^{-1} , respectively. Considering that the conductivity of a 100 nm thick film of commercial “conductive grade” **PEDOT:PSS** is 1 S cm^{-1} (Sigma Aldrich), these polymers clearly show promise as potential electrode or charge collection materials. Fig. 4a shows the cyclic voltammograms of 200 nm thick p-doped **PEDOT**, and neutral **PMT** and **PDMT** films deposited onto ITO-coated glass using chamber 1. Fig. 4b shows the cyclic voltammograms of 100 nm thick p-doped **PProDOT** and p-doped **PDMProDOT** deposited onto ITO-coated glass using chamber 2. Vapor deposited **PProDOT** and **PDMProDOT** films display comparable oxidation onset potentials and redox currents to **PEDOT** films, further suggesting that these films are suitable for electrochemical applications. Vapor deposited **PDMT** films display a higher oxidation potential compared to **PMT** films, corresponding to a deeper-lying HOMO band edge that is consistent with the behavior of the same polymer films obtained *via* electropolymerization. This shift in oxidation potential is attributed to reduced π -conjugation length due to the larger steric hindrance of **PDMT**.³⁵

The work function values and HOMO band edge positions of the vapor deposited polymers, as measured by UPS, are listed in Table 2. All UPS measurements were performed on ITO

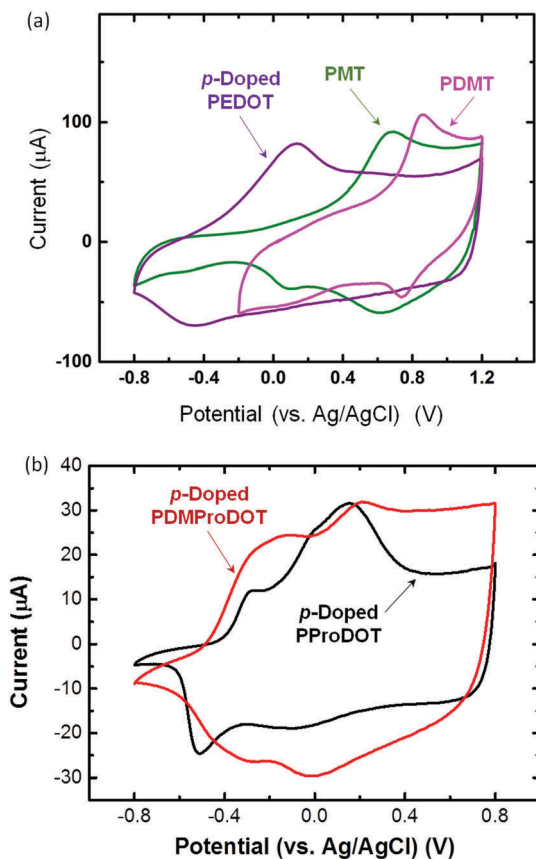


Fig. 4 (a) Cyclic voltammograms of 200 nm thick films of p-doped **PEDOT**, **PMT** and **PDMT** deposited onto ITO-covered glass using chamber 1 (FeCl_3 oxidant). (b) Cyclic voltammograms of 100 nm thick p-doped **PProDOT** and p-doped **PDMPProDOT** films deposited on ITO-covered glass using chamber 2 (FeCl_3 oxidant). Measurements were performed in 0.1 M tetrabutylammonium hexafluorophosphate (TBAF_6)/dichloromethane (DCM), with Ag/AgCl in acetonitrile as reference electrode.

substrates, the Fermi level of which was measured to be 4.5 eV. All the conducting polymers display Fermi levels that are up to 0.4 eV higher than that of PEDOT:PSS (5.1 eV).³⁶ The Fermi level of **PProDOT** changes from 4.94 eV to 4.90 and 4.76 eV after 10 s and 30 s of methanol rinsing, respectively, consistent with the absorption spectrum changes detailed in Fig. S4a (ESI[†]).

Vapor deposited **PBiT** and **PTerT** display HOMO band edge values similar to that of P3HT (5.1 eV). Notably, **PTT** shows a deep HOMO band edge (6.31 eV) after methanol rinsing. Fig. 5b shows the evolution of the **PTT** HOMO band edge position with

Table 2 Work functions and HOMO band edge positions of vapor deposited polymers

	Work function (eV)	Polymer	HOMO (eV)
PDMPProDOT	4.78	PBiT	4.98
PHMEDOT	5.02	PTerT	5.02
PProDOT (0 s ^a)	4.94	PTT (0 s)	6.39
PProDOT (10 s)	4.90	PTT (10 s)	6.29
PProDOT (30 s)	4.76	PTT (30 s)	6.21
		PTT (2 min)	6.31

^a Values in the brackets are rinsing times.

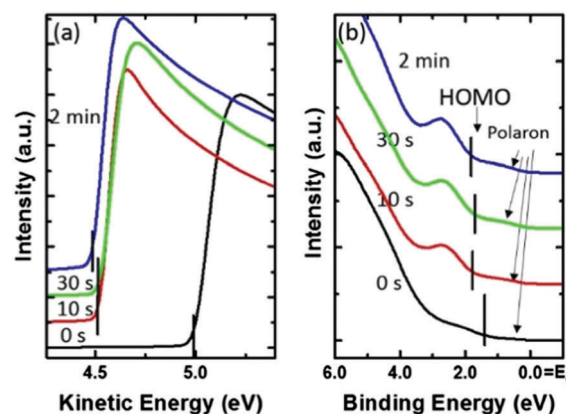


Fig. 5 Secondary electron cutoff (a) and binding energy corresponding to the substrate Fermi level (b) for vapor deposited **PTT** films (chamber 2, FeCl_3 oxidant) after different methanol rinsing times.

increasing methanol rinse times. The HOMO band edge of **PTT** changes from a starting level of 6.39 eV to 6.31 eV after 2 min of rinsing. The vacuum level changes by 0.5 eV after rinsing (Fig. 5a, 0 s versus 10 s). We ascribe the weak, low energy tails observed in Fig. 5b to a small residual population of p-doped **PTT** that is not removed by a methanol rinse.

4. Vapor coating of rough, highly-disordered substrates

Fig. 6a shows a photograph and an optical micrograph of a pre-woven linen textile coated with **PEDOT** in chamber 1, revealing a uniform (over multiple length scales), three-dimensional coating on both the entire 1×2 inch² sample and on each thread. Fig. 6b and c shows SEM images of the same textile before and after **PEDOT** coating. Each thread shown in the optical micrograph is comprised of microfibrils and a highly-conformal coating is formed on each microfibril.

Fig. 7 shows the optical micrographs and the corresponding SEM images of some highly disordered, high surface area substrates before (left column) and after vapor coating with p-doped **PEDOT** (right column) in chamber 1. The presence of **PEDOT** coatings on these substrates is evidenced by the dramatically different color of the pristine substrates compared to the **PEDOT**-coated substrates. A highly-conformal coating is formed over each small and large feature for all substrates. Further, a conformal coating can be achieved regardless of surface chemical composition or surface energy. The substrates shown in Fig. 7 include: paper (dominantly comprised of cellulose microfibrils), corduroy textile (58% polyester/42% rayon), and cotton towel. These three substrates were chosen to represent three different microstructures: paper has a characteristic rough, 2-dimensional surface; corduroy has micrometer sized wires sticking out from a main axis, forming a 3-dimensional meso-scale surface; and the cotton towel is a more complicated 3-dimensional surface containing many micron-sized wires that are either buried or highly twisted. Irrespective of the type of microstructure, highly-conformal **PEDOT** coatings can be readily achieved on all three substrates. **PEDOT** films are formed on all densely-packed wires in the corduroy textiles

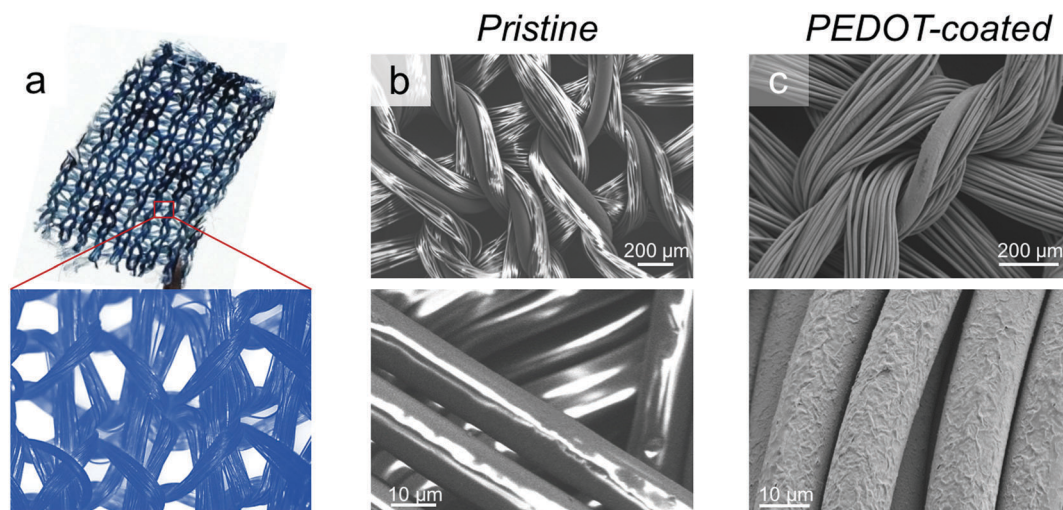


Fig. 6 (a) Picture (top) and optical micrograph (bottom) of a pre-woven linen textile coated with **PEDOT** in chamber 1. SEM images of pristine (b) and **PEDOT**-coated textiles (c).

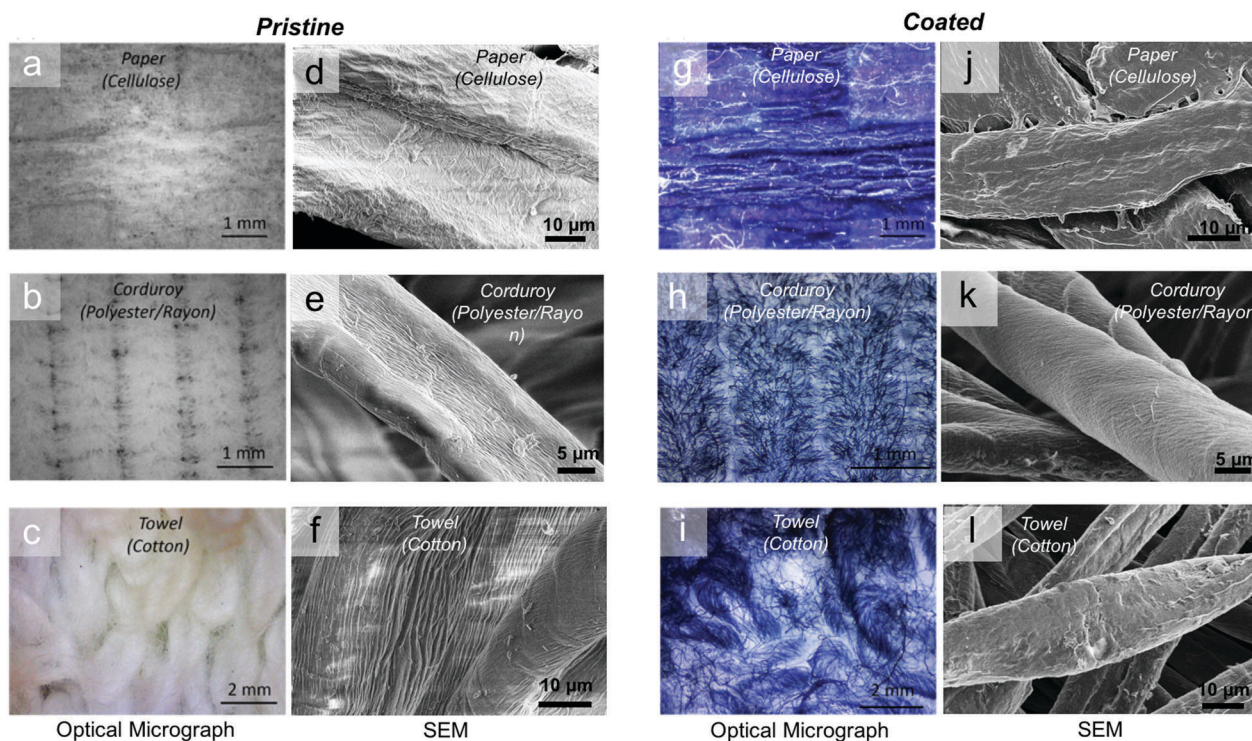


Fig. 7 Optical images (a–c and g–i) and SEM images (d–f and j–l) of pristine (left) and **PEDOT**-coated (right) paper, corduroy textile and cotton towel. All substrates were coated in chamber 1 using an FeCl_3 oxidant.

and the disordered, high surface area towel is also conformally coated by **PEDOT** films with high topographic fidelity.

Next, we confirmed that conformal coating of these three substrates can be achieved using either chamber 1 or chamber 2 to perform the deposition. Fig. 8 shows the optical micrographs (left column) and SEM images (right column) of the aforementioned substrates coated with **PTT** using chamber 2. The optical micrographs reveal that the salmon/orange-colored **PTT** is coated on the substrates uniformly. The SEM images

support the conformality of the polymer films on the various surfaces. The morphology of the **PTT** coated surfaces are slightly changed after coating. For example, the wrinkles on the surface of the pristine paper and textiles are covered by smooth polymer films.

We compared the vapor deposited **PEDOT** coating with solution processed **PEDOT:PSS** coatings. It is impossible to conformally and uniformly coat microstructured surfaces with conjugated polymers *via* solution processed routes because of

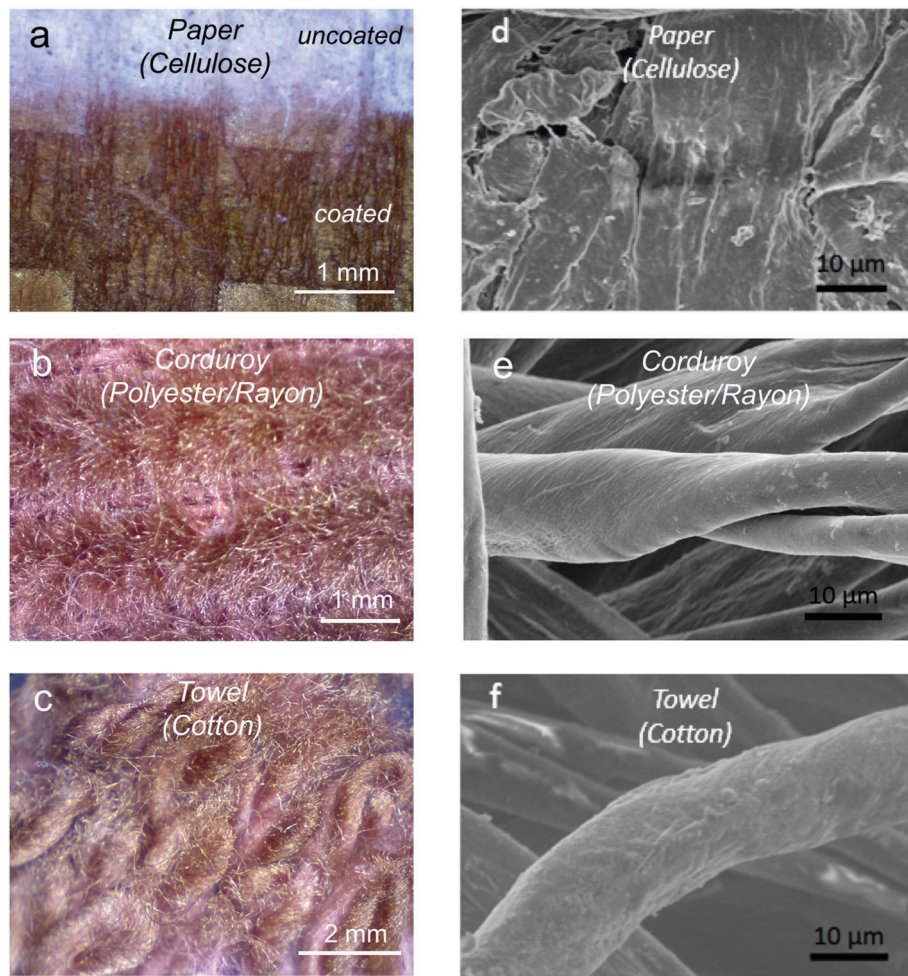


Fig. 8 Optical micrographs (a–c, left column) and SEM images (d–f, right column) of **PTT**-coated paper, corduroy textile and cotton towel. All substrates were coated in chamber 2.

irregular wetting, surface tension issues and flow-induced crystallization. Fig. 9a shows a photograph of corduroy coated with either **PEDOT**:PSS by spin-coating or **PEDOT** by vapor deposition in chamber 1. It is clear that spincoating does not produce a uniform coating over the entire area of the substrate, whereas vapor deposition yields a uniform **PEDOT** coating over the entire microstructured surface of the 2×2 inch corduroy sample. To assess differences between the coating morphologies of vapor deposited films to those obtained by dipcoating (*i.e.*, dyeing), we compared a cotton towel dipcoated with P3HT (10 mg mL^{-1} dichloromethane solution) to the **PTT** coated sample shown in Fig. 8f. Even though dipcoating seems to produce a uniform, polymer coated/infused fabric swatch (see Fig. S5, ESI[†]) to the naked eye, the SEM images in Fig. 9c reveal that random polymer agglomerations (due to flow-induced crystallization of polymer chains³⁷) and a non-uniform coating is produced by dipcoating, whereas **PTT** coated fibrils display smooth coatings.

Both vapor deposited **PEDOT** and **PTT** films obtained on paper and fabrics using chamber 1 and chamber 2, respectively, were observed to be physically robust and resistant to

mechanical washing. The **PEDOT** and **PTT** coatings were observed (by the naked eye) to remain on the cotton towel after rubbing or scraping, and numerous bending/twisting cycles. The surface sheet resistance of the **PEDOT**-coated prewoven linen textile shown in Fig. 6a was found to decrease by less than 5% after abrasion, folding (creasing), and 500 bending cycles (see Fig. 9b). The absorbance of the **PTT**-coated paper shown in Fig. 8a decreased less than 5% after rubbing 100 times. The absorbance of the **PTT**-coated cotton towel shown in Fig. 8c decreased by less than 10% after being soaked in either water or dichloromethane then dried. These results confirm that the vapor deposited films reported herein are mechanically robust.

Conclusions

A structurally-diverse set of conjugated monomers are polymerized *via* oxidative polymerization in the vapor phase. Two different reactive chambers in which to perform these vapor phase polymerizations are reported. One chamber boasts the ability to monitor film forming processes in real time but can

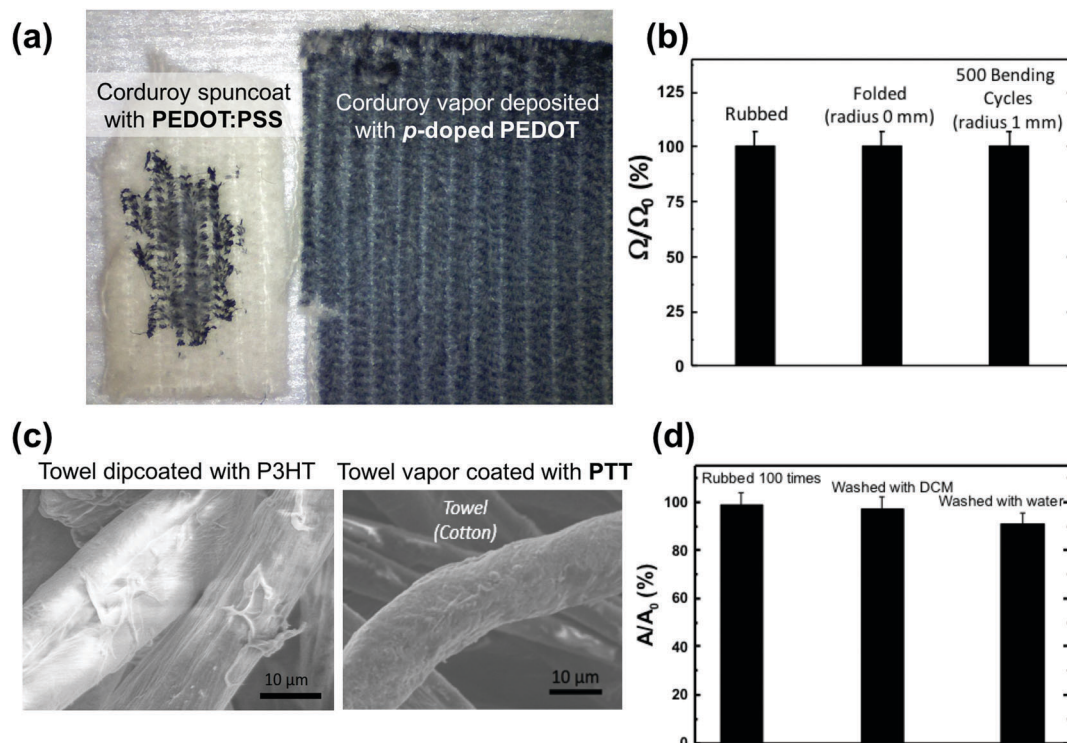


Fig. 9 (a) Photograph of (left) a 1 × 2 inch corduroy swatch coated with PEDOT:PSS via spincoating and (right) a 2 × 2 inch corduroy swatch vapor coated with p-doped PEDOT in chamber 1. (b) Change in surface sheet resistance measured for the PEDOT-coated linen textile shown in Fig. 6a after exposure to various mechanical stresses. (c) SEM image of a cotton towel dipcoated with poly(3-hexylthiophene) from dichloromethane (left) and a cotton towel vapor coated with PTT in chamber 2 (right). (d) Change in absorbance of a PTT-coated paper after rubbing and in a PTT-coated towel after washing with either water or dichloromethane.

only be used with high vapor pressure monomers. The second chamber lacks sophisticated *in situ* monitors but can be used with any monomer (solid or liquid) to produce conjugated polymer films. The reported vapor polymerization method is a strong alternative to common polymerization techniques, such as standard chemical synthesis and electrochemical polymerization. Selected conjugated polymer films obtained *via* vapor polymerization display unique electronic features that are not replicated in similar electrochemically polymerized or chemically polymerized counterparts. Notably, vapor deposited conjugated polymer films demonstrate the ability to uniformly and conformally coat rough, highly textured, high surface area substrates of diverse surface compositions and surface roughnesses. This feature will allow for bottom-up fabrication of flexible and wearable devices and textile-based electronic devices in which the active layers are directly and monolithically integrated onto a substrate surface.

Acknowledgements

The authors gratefully acknowledge financial support from the US Air Force Office of Scientific Research, under Agreement number FA9550-14-1-0128. T. L. A. also gratefully acknowledges partial support by the David and Lucille Packard Foundation.

Notes and references

- M. Kaltenbrunner, M. S. White, E. D. Glowacki, T. Sekitani, T. Someya, N. S. Sariciftci and S. Bauer, *Nat. Commun.*, 2012, **3**, 770–776.
- S. Savagatrup, A. D. Printz, T. F. O'Connor, A. V. Zaretski and D. J. Lipomi, *Chem. Mater.*, 2014, **26**, 3028–3041.
- J. Y. Lee, S. T. Connor, Y. Cui and P. Peumans, *Nano Lett.*, 2010, **10**, 1276.
- M. Kaltenbrunner, T. Sekitani, J. Reeder, T. Yokota, K. Kuribara, T. Tokuhara, M. Drack, R. Schwodiauer, I. Graz, S. Bauer-Gogonea, S. Bauer and T. Someya, *Nature*, 2013, **499**, 458–463.
- O. Awartani, B. Lemanski, H. W. Ro, L. J. Richter, D. M. DeLongchamp and B. T. O'Connor, *Adv. Energy Mater.*, 2013, **3**, 399–406.
- G. Schwartz, B. C.-K. Tee, J. Mei, A. L. Appleton, D. H. Kim, H. Wang and Z. Bao, *Nat. Commun.*, 2013, **4**, 1859.
- M. C. Barr, J. A. Rowehl, R. R. Lunt, J. Xu, A. Wang, C. M. Boyce, S. G. Im, V. Bulović and K. K. Gleason, *Adv. Mater.*, 2011, **23**, 3500–3505.
- M. S. White, M. Kaltenbrunner, E. D. Glowacki, K. Gutnichenko, G. Kettlgruber, I. Graz, S. Aazou, C. Ulbricht, D. A. M. Egbe, M. C. Miron, Z. Major, M. Scharber, T. Sekitani, T. Someya, S. Bauer and N. S. Sariciftci, *Nat. Photonics*, 2013, **7**, 811–816.

- 9 D. J. Lipomi, B. C.-K. Tee, M. Vosgueritchian and Z. N. Bao, *Adv. Mater.*, 2011, **23**, 1771–1775.
- 10 T. F. O'Connor, A. V. Zaretski, S. Savagatrup, A. D. Printz, C. D. Wilkes, M. I. Diaz, E. J. Swayer and D. J. Lipomi, *Sol. Energy Mater. Sol. Cells*, 2016, **144**, 438–444.
- 11 L. Dou, Y. Liu, Z. Hong, G. Li and Y. Yang, *Chem. Rev.*, 2015, **115**, 12633–12665; P. M. Beaujuge and J. R. Reynolds, *Chem. Rev.*, 2010, **110**, 268–320; X. Guo, A. Facchetti and T. J. Marks, *Chem. Rev.*, 2014, **114**, 8943–9021.
- 12 D. Choi, M. Chang and E. Reichmanis, *Adv. Funct. Mater.*, 2014, **25**, 920–927.
- 13 T. P. Martin, A. J. Wise, E. Busby, J. Gao, M. J. Ford, A. J. Moulé, S. D. Larsen and J. K. Grey, *J. Phys. Chem. B*, 2013, **117**, 4478–4487; Y. Gao, T. P. Martin, E. T. Niles, A. K. Thomas, A. J. Wise and J. K. Grey, *J. Phys. Chem. C*, 2010, **114**, 15121–15128.
- 14 C. R. McNeill, *Energy Environ. Sci.*, 2012, **5**, 5653–5667.
- 15 K. Jost, C. R. Perez, J. K. McDonough, V. Presser, M. Heon, G. Dion and Y. Gogotsi, *Energy Environ. Sci.*, 2011, **4**, 5060–5067; L. B. Hu, M. Pasta, F. L. Mantia, L. F. Cui, S. Jeong, H. D. Deshazer, J. W. Choi, S. M. Han and Y. Cui, *Nano Lett.*, 2010, **10**, 708–714.
- 16 K. Jost, G. Dion and Y. Gogotsi, *J. Mater. Chem. A*, 2014, **2**, 10776–10787.
- 17 J. Bae, M. K. Song, Y. J. Park, J. M. Kim, M. L. Liu and Z. L. Wang, *Angew. Chem., Int. Ed.*, 2011, **50**, 1683–1687; Y. Fu, X. Cai, H. Wu, Z. Lv, S. Hou, M. Peng, X. Yu and D. Zou, *Adv. Mater.*, 2012, **24**, 5713–5718; C. Das, B. Jain and K. Krishnamoorthy, *Chem. Commun.*, 2015, **51**, 11662–11664.
- 18 Y. Ding, M. A. Invernale and G. A. Sotzing, *ACS Appl. Mater. Interfaces*, 2010, **2**, 1588–1593; C. Yeon, G. Kim, J. W. Lim and S. J. Yun, *RSC Adv.*, 2017, **7**, 5888–5897; J. D. Ryan, D. A. Mengistie, R. Gabrielsson, A. Lund and C. Müller, *ACS Appl. Mater. Interfaces*, 2017, **9**, 9045–9050; Y. Du, K. Cai, S. Chen, H. Wang, S. Z. Shen, R. Donelson and T. Lin, *Sci. Rep.*, 2015, **5**, 6411.
- 19 K. Hong, K. Oh and T. Kang, *J. Appl. Polym. Sci.*, 2005, **97**, 1326–1332; J. Xu, D. Wang, L. Fan, Y. Yuan, W. Wei, R. Liu, S. Gu and W. Xu, *Org. Electron.*, 2015, **26**, 292–299; N. Maráková, P. Humpolíček, V. Kašpárková, Z. Capáková, L. Martinková, P. Bober, M. Trchová and J. Stejskal, *Appl. Surf. Sci.*, 2017, **396**, 169–176.
- 20 J. Yatvin, S. A. Sherman, S. F. Filocamo and J. Locklin, *Polym. Chem.*, 2015, **6**, 3090–3097.
- 21 B. Lin, R. Sureshkumar and J. L. Kardos, *Chem. Eng. Sci.*, 2001, **56**, 6563–6575; S. Y. Severt, N. A. Ostrovsky-Snider, J. M. Leger and A. R. Murphy, *ACS Appl. Mater. Interfaces*, 2015, **7**, 25281–25288; S. Sadki, P. Schottland, N. Brodie and G. Sabouraud, *Chem. Soc. Rev.*, 2000, **29**, 283–293.
- 22 C. Musumeci, J. A. Hutchison and P. Samori, *Nanoscale*, 2013, **5**, 7756–7761.
- 23 M. Åkerfeldt, M. Strååt and P. Walkenström, *Text. Res. J.*, 2013, **83**, 2164–2176.
- 24 M. R. Lee, R. D. Eckert, K. Forberich, G. Dennler, C. J. Brabec and R. A. Gaudiana, *Science*, 2009, **324**, 232–235.
- 25 S. M. George, *Chem. Rev.*, 2010, **110**, 111–131.
- 26 K. M. Vaeth and K. F. Jensen, *Adv. Mater.*, 1999, **11**, 814–820.
- 27 K. K. S. Lau and K. K. Gleason, *Macromolecules*, 2006, **39**, 3688–3694.
- 28 D. Bhattacharyya, R. M. Howden, D. C. Borrelli and K. K. Gleason, *J. Polym. Sci., Part B: Polym. Phys.*, 2012, **50**, 1329–1351.
- 29 H. Nishimura and J. Mizutani, *J. Org. Chem.*, 1975, **40**, 1567–1575.
- 30 W. E. Tenhaeff and K. K. Gleason, *Adv. Funct. Mater.*, 2008, **18**, 979–992; A. M. Coclite, R. M. Howden, D. C. Borrelli, C. D. Petruczuk, R. Yang, J. L. Yagüe, A. Ugur, N. Chen, S. Lee, W. J. Jo, A. Liu, X. Wang and K. K. Gleason, *Adv. Mater.*, 2013, **25**, 5392–5423.
- 31 S. G. Im and K. K. Gleason, *Appl. Phys. Lett.*, 2007, **90**, 152112.
- 32 T. D. McCarley, C. O. Noble, IV, C. J. DuBois, Jr. and R. L. McCarley, *Macromolecules*, 2001, **34**, 7999–8004.
- 33 H. Goktas, X. Wang, N. D. Boscher, S. Torosian and K. K. Gleason, *J. Mater. Chem. C*, 2016, **4**, 3403–3414.
- 34 H. Meier, U. Stalmach and H. Kolshorn, *Acta Polym.*, 1997, **48**, 379–384.
- 35 S. Lagoutte, P.-H. Aubert, F. Tran-Van, X. Sallenave, C. Laffaiteur, C. Sarrazin and C. Chevrot, *Electrochim. Acta*, 2013, **106**, 13–22.
- 36 O. Bubnova, Z. U. Khan, H. Wang, S. Braun, D. R. Evans, M. Fabretto, P. Hojati-Talemi, D. Dagnelund, J.-B. Arlin, Y. H. Geerts, S. Desbief, D. W. Breiby, J. W. Andreasen, R. Lazzaroni, W. M. Chen, I. Zozoulenko, M. Fahlman, P. J. Murphy, M. Berggren and X. Crispin, *Nat. Mater.*, 2014, **13**, 190–194.
- 37 Y. Diao, Y. Zhou, T. Kurosawa, L. Shaw, C. Wang, S. Park, Y. Guo, J. A. Reinspach, K. Gu, X. Gu, B. C. K. Tee, C. Pang, H. Yan, D. Zhao, M. F. Toney, S. C. B. Mannsfeld and Z. Bao, *Nat. Commun.*, 2015, **6**, 7955.